Original Investigation

CT Radiomics Signature of Tumor and Peritumoral Lung Parenchyma to Predict Nonsmall Cell Lung Cancer Postsurgical Recurrence Risk

Tugba Akinci D'Antonoli, MD, Alessandra Farchione, MD, PhD, Jacopo Lenkowicz, MSc, Marco Chiappetta, MD, Giuseppe Cicchetti, MD, Antonella Martino, MD, Alessandra Ottavianelli, MD, Riccardo Manfredi, MD, Stefano Margaritora, MD, Lorenzo Bonomo, MD, Vincenzo Valentini, MD, Anna Rita Larici, MD

Abbreviations

NSCLC nonsmall cell lung cancer

CT computed tomography

TNM tumor-node-metastasis

DICOM Digital Imaging and Communication in Medicine

ROI region of interest

IQR interquartile range

ROC receiving operator characteristic

AUC area under the curve

AIC Akaike information criteria

OR odds ratio

CI confidence interval

Rad-score radiomics signature based score

Rationale and Objectives: To estimate recurrence risk after surgery in nonsmall cell lung cancer (NSCLC) patients by employing tumoral and peritumoral radiomics analysis.

Materials and Methods: One-hundred twenty-four surgically treated stage IA–IIB NSCLC patients' data from 2008 to 2013 were retrospectively collected. Patient outcome was defined as local recurrence (LR), distant metastasis (DM), and (sum of LR and DM) total recurrence (TR) at follow-up. Volumetric region of interests (ROIs) were drawn for the tumor, peritumoral lung parenchyma (2 cm around the tumor) and involved lobe on CT images. Ninety-four (morphological, first-order, textural, fractal-based) radiomics features were extracted from the ROIs and datasets were created from single or combined ROIs. Predictive models were built with radiomics signature (RS) and clinicopathological data, and the area under the curve (AUC) was used to evaluate the performance. Radiomics score was calculated with the best models' feature coefficients, low- and high-risk groups of patients defined accordingly. Kaplan–Meier curves were built, and the log-rank test was used for comparison among low- and high-risk groups. Differences in recurrence risk among the two risk groups were calculated (chi-square test).

Results: Fifty-six patients developed TR (25 LR, 31 DM). The tumor-node-metastasis (TNM) stage recurrence predictability (AUC_{TR} 0.680; AUC_{DM} 0.672; AUC_{LR} 0.580) was substantially improved when RS was added to the predictive model (AUC_{TR} 0.760; AUC_{DM} 0.759; AUC_{LR} 0.750). Seventy-five percent of high-risk patients developed TR. Recurrence risk of the high-risk group was 16-fold higher than that of the low-risk group ($p < 0.001$).

Conclusion: Combination of the tumoral and peritumoral RS with TNM staging system outperformed TNM staging alone in individualized recurrence risk estimation of patients with surgically treated NSCLC.

Key Words: Lung neoplasms; Multidetector computed tomography; Radiomics; Nomograms; Prognosis.

Acad Radiol 2019; ■:1–11

From the Istituto di Radiologia, Università Cattolica del Sacro Cuore, Largo Francesco Vito 1, 00168, Rome, Italy (T.A.D., J.L., G.C., A.M., A.O., R.M., V.V., A.R.L.); Dipartimento Diagnostica per Immagini, Radioterapia Oncologica ed Ematologia, Fondazione Policlinico Universitario "A. Gemelli" IRCCS, Rome, Italy (T.A.D., A.F., G.C., A.O., R.M., L.B., V.V., A.R.L.); Clinic of Radiology and Nuclear Medicine, University Hospital Basel, University of Basel, Basel, Switzerland (T.A.D.); Dipartimento Scienze Cardiovascolari e Chirurgiche, Fondazione Policlinico Universitario "A. Gemelli" IRCCS, Rome, Italy (M.C., S.M.); Istituto di Patologia Speciale Chirurgica, Università Cattolica del Sacro Cuore, Rome, Italy (S.M.). Received May 3, 2019; revised May 24, 2019; accepted May 28, 2019. **Address correspondence to:** Jacopo Lenkowicz. e-mail: jacopo.lenkowicz@gmail.com

https://doi.org/10.1016/j.acra.2019.05.019

RS
radiomics signature
LR
local recurrence
DM
distant metastasis
TR
total recurrence

INTRODUCTION

Lung cancer is the leading cause of cancer-related deaths worldwide, and nonsmall cell lung cancer (NSCLC) is the most common histological type (1). Surgery is the curative treatment for the early-stage disease (stage I and II) and locally advanced disease (stage IIIA) with resectable N2 or T4 tumor without nodal involvement (2). Despite early diagnosis or complete resection, NSCLC recurrence is the most common cause of death and deterioration of life quality (2,3). Defining the recurrence risk at the time of diagnosis would allow tailoring patient's treatment and, therefore, improving patient's survival (4).

Preoperative conventional imaging methods are crucial for tumor-node-metastasis (TNM) stage determination, which is traditionally used for assessing the treatment response or survival. However, the prognosis of the NSCLC remains mostly uncertain at the time of diagnosis (2,3). Radiomics refers to extracting quantitative features from images and turning them into mineable data, which has the potential to decipher tumor histopathology and behavior, and to predict patient's prognosis in a noninvasive manner (5). Several studies focused on recurrence prediction by using the radiomics analysis of tumor in patients with NSCLC (6–9). Combination of the radiomics signature (RS) with TNM stage and other clinicopathological (CP) data demonstrated better performance than TNM staging alone in estimating disease-free-survival in patients with early-stage NSCLC (6).

Tumor spread into the surrounding tissues is mostly responsible for worse survival and tumor recurrence (3). Radiologically defined peritumoral semantic features (peritumoral interstitial thickening and tumor margin characteristics) on computed tomography (CT) were found positively correlated with recurrence in NSCLC patients (3). Combination of peritumoral semantic features and tumoral radiomics features improved accuracy in predicting lymph node metastasis of lung adenocarcinoma (10). Pretreatment peritumoral lung parenchyma radiomics analysis of the 3 mm tissue around the tumor on CT and of the voxels immediately surrounding the tumor on positron emission tomography were found predictive for distant metastasis in patients with locally advanced and early-stage NSCLC, respectively (11,12). However, to the best of our knowledge, radiomics analysis of peritumoral lung parenchyma 2 cm away from the tumor contour, which is defined as the safe surgical margin (13, in NSCLC patients undergoing surgery has not been performed previously, and its relevance in predicting the risk of recurrence via radiomics score has not been evaluated.

We aimed to develop a predictive model for recurrence risk in NSCLC patients by combining CP risk factors with tumoral and peritumoral RS extracted from presurgical CT images. Our secondary aim was to develop a multiparametric nomogram to assess how the predictive model performed over TNM staging.

MATERIALS AND METHODS

Patient Population and Tumor Characteristics

This study was conducted under an institutional review board approved protocol (ADV.AN.CE = ADVanced imaging ANalysis in lung nodule and CancEr) with a waiver of patient informed consent for retrospective studies.

Surgically treated stage IA to IIB NSCLC patients' data in our institution from January 2008 to December 2013 were retrospectively collected. At pathological staging, 16 patients were upstaged to IIIA; those patients, therefore, received adjuvant chemo-/radiotherapy after surgery.

Tumor staging was performed according to the current TNM staging system at the time of the analysis (7th edition) (14). Inclusion and exclusion criteria are shown in Figure 1, along with recruitment pathway. According to our institution's protocol, patients were followed up with clinical examinations, blood test analysis, and head-chest-abdomen CT every six months for the first five years after surgery, then annually.

Surgery was performed through a thoracotomy or video-assisted thoracoscopic surgery. All patients underwent tumor resection (lobectomy, bilobectomy, pneumonectomy, or sublobar resection) with lymph node sampling or mediastinal lymph node dissection according to existing guidelines (15). Lobectomy is the standard of care for NSCLC; however, early stages of disease could be successfully treated with sublobar resection (2,16).

Demographic and CP data (age, sex, smoking status, histopathology, TNM stage) were collected from medical archives. Tumor recurrence was determined on follow-up CT examinations. Total recurrence (TR) was defined as the sum of local recurrence (LR) and distant metastasis (DM) outcomes. LR was described as chest recurrence, located either at the surgical margin (parenchymal, pleural, bronchial stump) or at ipsilateral hilar/mediastinal lymph nodes, DM was considered as all the other recurrences.

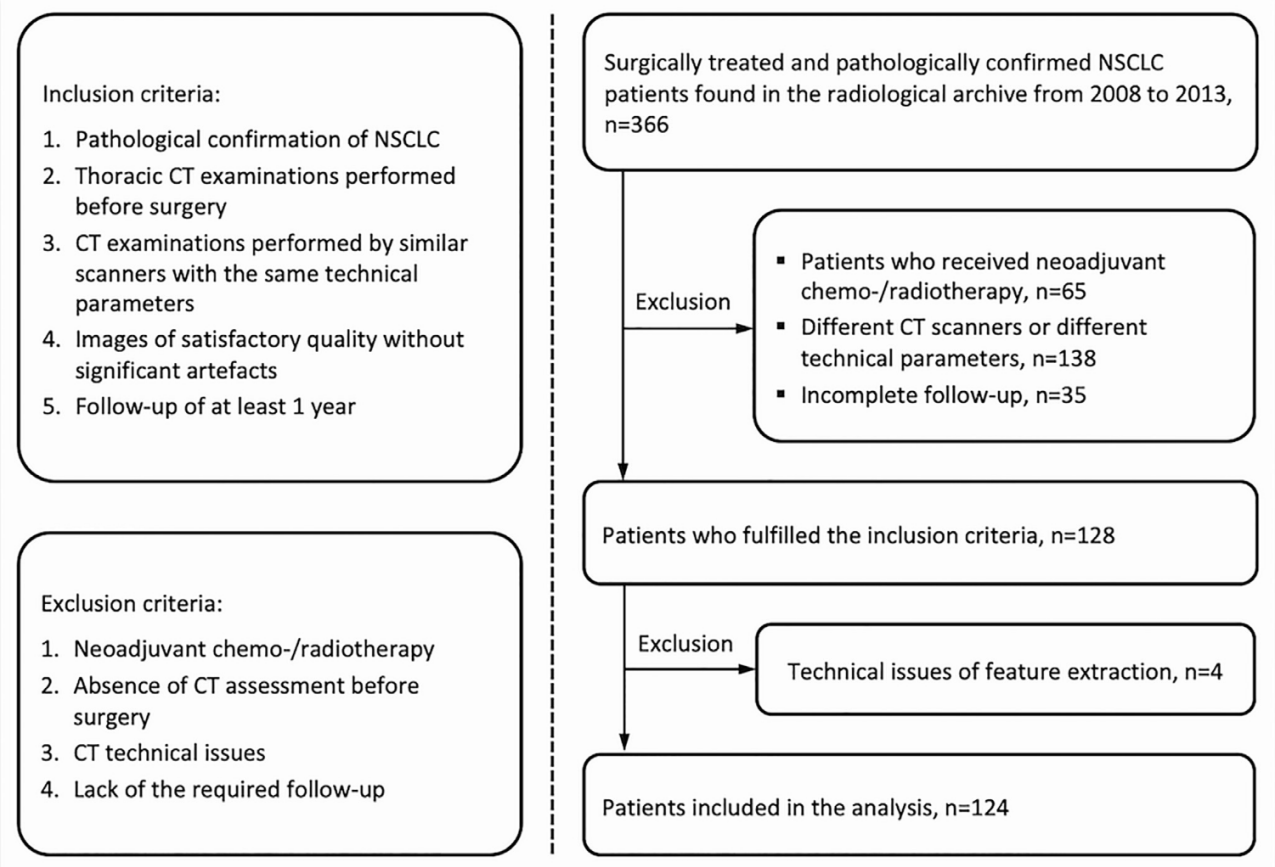

Figure 1. Recruitment pathway of the study.

CT Protocol

Chest CT scan alone or included in the head-chest-abdomen CT examination, were considered. Imaging was performed with a median of 1 (interquartile range [IQR] 0−2) month before surgery. CT acquisition and reconstruction parameters are summarized in Table 1. To improve reproducibility (17,18) we selected the studies that have the same CT acquisition/reconstruction parameters (slice thickness of 2.5 mm and standard kernel). Contrast-enhanced images were used for the analysis because they were available for all cases.

Image Analysis

Images were uploaded on a radiotherapy delineation console (Eclipse, Varian Medical Systems, Palo Alto, CA) for region of interest (ROI) definition. A fellow in chest radiology with 5 years of experience (T.A.D.) was responsible for tumor segmentation. A slice-by-slice semi-automatic segmentation system (computer-aided edge detection followed by manual delineation) was used to improve reproducibility (5,19−23). All contours were approved by two chest radiologists with 18 and 5 years of experience (A.R.L., A.F.), respectively. The segmentation process was started on mediastinal window setting (width: 450 HU; level: 50 HU) to separate the tumor from the adjacent structures, and completed on lung window setting (width: 1600 HU; level: −600 HU) to adjust the selected ROI to the tumor margins more precisely.

Three-dimensional volumetric ROIs were defined for each patient: (1) gross tumoral volume (GTV), (2) peritumoral volume (PTV), including the lung parenchyma 2 cm away from the tumor contour, and (3) volume of the entire lobe (LBV) where the tumor was located (Fig. 2). The peritumor zone was defined as the lung parenchyma within 2 cm of lung tumor because this threshold is usually considered the safe margin for limited or sublobar lung resection (segmentectomy and wedge resection) when appropriate (13). Entire lobe was delineated to extend the analysis into the surgical standard-of-care area (2).

The analysis was performed by using an in-house developed free and open-source software, named *Moddicom*, which implemented by a multidisciplinary biotechnology innovation group and validated in an international multicentric project (24,25). Digital imaging and communication in medicine files containing the images were used for the delineation and the voxel structure sets with contour coordinates were uploaded to software for analysis. A Laplacian of Gaussian convolution kernel filter (σ range 0.3−3, in incremental steps of 0.01) was employed to decrease noise and enhance features at different spatial scales (19). Ninety-four radiomics features (15 morphological, 17 first-order statistical, 57 textural, and 5 fractal-based) were extracted from

TABLE 1. CT Acquisition and Reconstruction Parameters

CT acquisition parameters	
Equipment	64-row MDCT (Light Speed VCT XT), 16-row MDCT (Light Speed Pro) (GE Healthcare, Milwaukee, WI)
Acquisition type	Helical
Tube	120 kV
Rotation time	0.5 s
Auto mA	Yes
Collimation	64 × 0.625 mm, 16 × 1.25 mm
Orientation	Supine, craniocaudal, inspiratory breath-hold
Dose reduction	Z-axis automatic tube current modulation technique
Scan reconstruction parameters	
Slice thickness/kernel	2.5 mm/standard (mediastinum)
Reconstruction interval	2.5 mm
Window/level	450/50 HU (mediastinum)
Matrix	512 × 512
Contrast medium administration protocol	
Preparation	20-Gauge needle inserted into a brachial vein
Injection rate	3 mL/s
Injector	Power injector (Medrad Stellant Dual Head Injector; Medrad, Warrendale, PA)
Contrast volume and type	90–140 mL (according to patient's BMI) of nonionic iodine contrast medium, concentration of 350 mg/mL (Iomeron, Bracco, Milan, Italy), 370 mg/mL (Ultravist, Bayer Healthcare, Berlin, Germany), or 400 mg/mL (Iomeron, Bracco, Milan, Italy)
Scan delay	35–40 s (arterial phase) or 70/75 s (portal phase)

BMI, body mass index; HU, Hounsfield unit; kV, kilovoltage; mA, milliampere; MDCT, multidetector computed tomography; mg, milligram; mL, milliliter; s, second.

each delineated ROI on Laplacian of Gaussian filtered and unfiltered images. List of all extracted features, source code, and data published in a public repository (https://github.com/kbolab/LungRecurrence).

Statistical Analysis

Descriptive Statistics

Comparisons of patient and tumor characteristics were conducted by a two-sample *t* test for continuous variables, contingency tables, and Fisher's exact test for categorical variables.

Radiomics Signature and Score

A dataset for each ROI combination (i.e., GTV, PTV, LBV, GTV+PTV, GTV+LBV, GTV+PTV+LBV) was built with

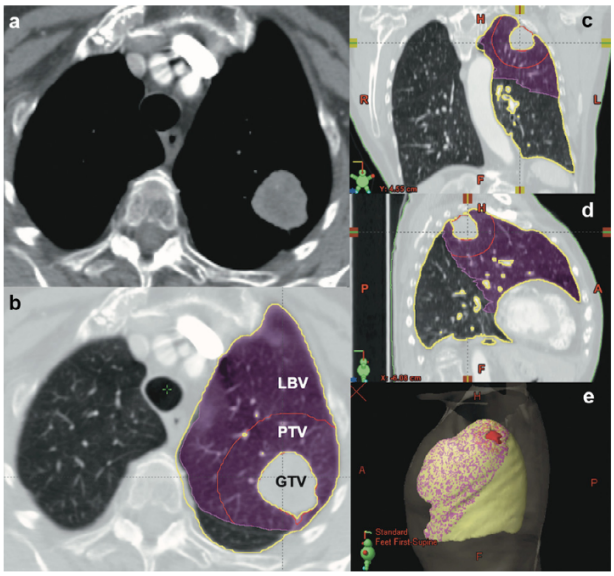

Figure 2. The segmentation of the 3D region of interests (ROIs) was started on axial CT images with mediastinal window setting (a) to separate the tumor from the adjacent structures, and completed on axial images with lung window setting (b) to adjust the selected ROI to the tumor margins more precisely. The 3 ROIs were defined for the tumor volume (gross tumoral volume, GTV), the peritumor zone volume (peritumoral volume, PTV), delineated 2 cm away from the tumor contour, and the lobe volume (lobar volume, LBV), delineated for the entire lobe where the tumor was located. Coronal (c), sagittal (d) and volumetric (e) images show the extension of volumetric ROIs. Axial CT scan with a mediastinal window setting demonstrates the tumor heterogeneity.

filtered and unfiltered radiomics features. The feature selection was performed in three steps: First, for each dataset, univariate correlation test concerning the clinical outcomes was conducted with Mann-Whitney *U* test, the features with a significant level of correlation ($p$value < 0.05) were selected. Second, 10-fold cross-validation was performed by using the "fscaret" R package (26) to select the top performing features for each different ROI combination. The number of selected features was limited to 10 to avoid overfitting (27). Lastly, these six sets of features were put in a Cox proportional-hazard model, and through stepwise selection based on Akaike information criteria (AIC), a single final model for each ROI combination was selected. Model validation was performed with repeated 10-fold cross-validation, and the models were evaluated with the receiving operator characteristic (ROC) curves and their area under the curve (AUC) values. The model with the highest AUC was selected as the overall final model. The entire process was repeated for each clinical outcome (i.e., LR, TR, and DM).

A radiomics signature based score (Rad-score) for each outcome was then built from the final model features weighted by their coefficients. The Rad-score cut-off values to define low- and high-risk groups were chosen according to the Youden index criterion (28). Kaplan-Meier curves were stratified in low- and high-risk according to the Rad-score were built for each CP covariate. The log-rank test was

used to assess the recurrence outcome difference between low- and high-risk patients. Differences in recurrence risk among the two risk groups were calculated (chi-square test) and odds ratios (OR) were computed.

Combined Predictive Models and Comparison

The CP data were chosen among pathological TNM (pTNM) stage, histopathology (adenocarcinoma: yes/no), age (≤60 or >60 years), type of surgery (lobectomy: yes/no), smoking status (yes/no), sex (male/female), and tumor structure (solid/subsolid). Cox proportional-hazard models including only CP data and only RS data were separately built through step-wise selection based on AIC minimization; then, in order to build a third model, with CP+RS, the CP-only model predictors were added to the previously defined RS features. Among these three models (CP-only, RS-only, CP+RS) the best was chosen according to minimal AIC and DeLong's test on ROC curves' AUC from repeated 10-fold cross-validation. Nomograms were built at 1-, 2-, and 3-year end-points for each outcome to demonstrate the incremental value of RS to the TNM stage in individualized recurrence risk. Calibration plots at 1-, 2-, 3-year end-points were drawn to compare agreement and ensure the reliability of the nomograms. All statistical analyses were performed with R software version 3.3.2 (https://www.r-project.org) and "fscaret" package (26). The statistical significance level was accepted as $p < 0.05$.

RESULTS

Patient Population and Tumor Characteristics

The study population consisted of 124 surgically treated patients. The characteristics of patients and tumors are summarized in Table 2 according to their recurrence status. The median age was 68 years (IQR 59.5−75), 73 (59%) patients were male, 85 (69%) patients were current or former smokers, and the median smoking pack/years were 23 (IQR 15−45). No significant difference was found between recurrence and nonrecurrence group according to patient's age, smoking history, sex (*t* test $p = 0.93$; Fisher's exact test $p = 0.88$, 0.71, respectively). Fifty-six (45%) patients developed tumor recurrence after surgery: 25 (20%) LR and 31 (25%) DM. The median follow-up time was 57 (IQR 33.5−81) months and the median time-to-recurrence was 23.5 (IQR 11.5−32) months. Forty-two (34%) patients died during the follow-up, and the median time-to-death was 35.5 (IQR 23−47) months.

Fifty-seven (45%) patients had clinical stage IA disease, and 55 (44%) patients had pathological stage IA disease. Sixteen (12.9%) patients were upstaged to stage IIIA at pathology: 3 (2.4%) of them from clinical T3-N0 to pathological T4-N0 stage, 13 (10.5%) of them from clinical T1-N0, T2-N0, and T3-N0 to pathological T1-N2, T2-N2, and T3-N1 stage, respectively. Among those 16 patients, recurrence percentages were higher than the rest of the study population: 4 (25%) patients developed LR, 7 (44%) patients DM, and 5 (31%) patients had no recurrence. The main reason for upstaging was microscopic lymph node metastasis, and all N-upstaged patients developed recurrence.

TABLE 2. Patient and Tumor Characteristics ($n = 124$)

	No Recurrence $n = 68$	Total Recurrence $n = 56$	p Value
Age (mean ± SD)	66.54 ± 12.60	66.73 ± 9.87	0.93
Smoking status			0.88
Current or former smoker	47 (55.3)	38 (44.7)	
Nonsmoker	21 (53.9)	18 (46.1)	
Sex			0.71
Male	39 (53.4)	34 (46.6)	
Female	29 (56.9)	22 (43.1)	
Histopathology			0.69
Adenocarcinoma	50 (54.4)	42 (45.6)	
Squamous cell carcinoma	14 (60.9)	9 (39.1)	
Other nonsquamous neoplasia	4 (44.4)	5 (55.6)	
cTNM Stage			0.03*
IA	38 (66.6)	19 (33.4)	
IB	16 (57.2)	12 (42.8)	
IIA	8 (36.4)	14 (63.6)	
IIB	6 (35.3)	11 (64.7)	
pTNM stage			0.008*
IA	38 (69.1)	17 (30.9)	
IB	15 (62.5)	9 (37.5)	
IIA	7 (38.9)	11 (61.1)	
IIB	3 (31.3)	8 (68.7)	
IIIA	5 (27.3)	11 (72.7)	
pT			0.47
1a	23 (62.2)	15 (37.8)	
1b	15 (65.2)	8 (34.8)	
2a	17 (48.6)	18 (51.4)	
2b	7 (58.3)	5 (41.7)	
3	5 (38.5)	8 (61.5)	
4	1 (33.3)	2 (66.7)	
pN			0.001*
0	62 (63.3)	36 (36.7)	
1	4 (26.7)	11 (73.3)	
2	2 (18.2)	9 (81.8)	
Tumor structure			0.025*
Subsolid	21 (75)	7 (25)	
Solid	47 (49)	49 (51)	
Type of surgery			0.57
Lobectomy	56 (54.9)	46 (45.1)	
Bilobectomy	4 (80)	1 (20)	
Pneumonectomy	0 (0.0)	2 (100)	
Sublobar resection	8 (53.3)	7 (46.7)	

Numbers in parentheses are row percentages.

cTNM, clinical tumor-node-metastasis; n, number; pTNM, pathological tumor-node-metastasis; SD, standard deviation.

* Statistically significant at $p < 0.05$ (Fisher's exact test).

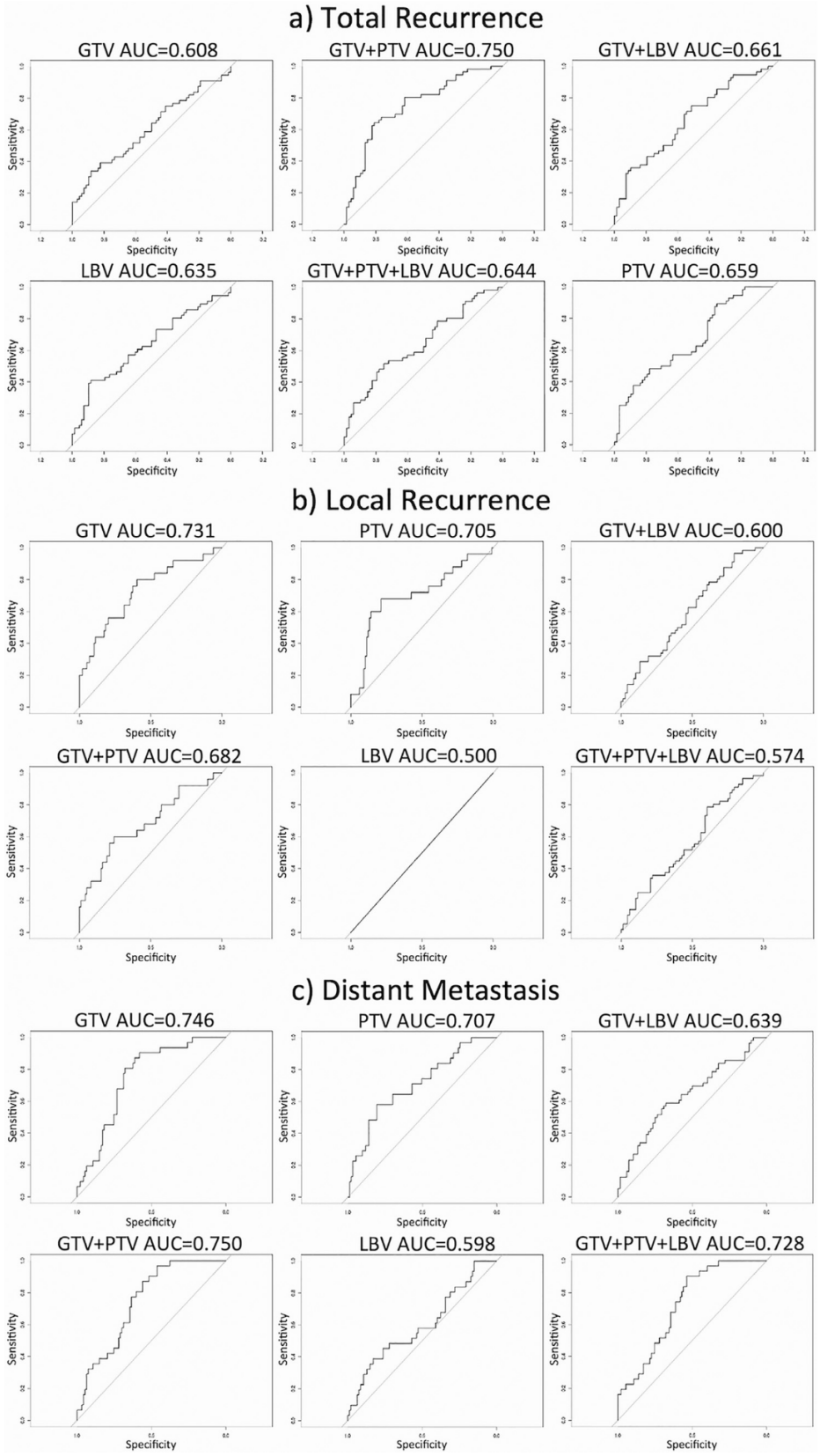

Figure 3. Graphics show the performance (ROC curves and AUC values) of the models obtained from different ROI combinations for each outcome (a) total recurrence, (b) local recurrence, (c) distant metastasis. Abbreviations: AUC, area under the curve; GTV, gross tumoral volume; LBV, lobar volume; PTV, peritumoral volume; ROI, region of interest.

Image and Statistical Analysis

Radiomics Signature and Score

The performance of the models created for different ROI combinations for each outcome is graphically shown in Figure 3. The best-performing model was observed with "GTV+PTV" dataset for TR and DM (AUC 0.750, for both) and with "GTV" dataset alone for LR (AUC 0.731) outcomes. The peritumoral "PTV" dataset alone also reached a fair level of performance in predicting LR (AUC 0.705) and DM (AUC 0.707) outcomes.

The Rad-score was computed from the textural, morphological, and intensity based features—which depicts tumor shape and heterogeneity—of the best performing models. The individual contribution of the selected features to the Rad-score construction is presented in Figure 4.

The Rad-score formula and Youden cut-off values are reported in Table 3. Patients were classified into low- and high-risk groups for recurrence, respectively above and below the cut-off values (TR = 9.68; LR = −14.9; DM = 22.09). Detailed feature and model descriptions are published in the public repository.

Sixty-one (49.1%) patients were assigned to the high-risk group, and among them, 46 (75.4%) developed recurrence at overall end-point. Sixty-three (50.9%) patients were assigned to the low-risk group, and among them, 10 (15.9%) developed recurrence at overall end-points. The high-risk group

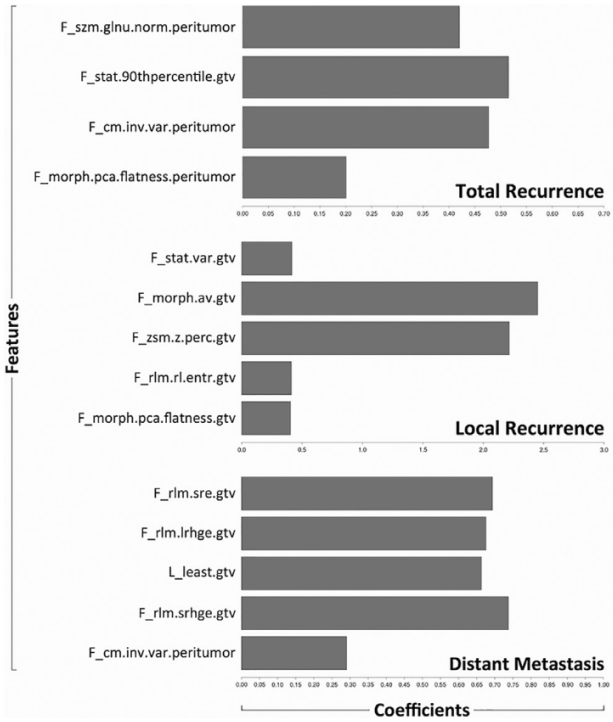

Figure 4. Histograms show the contribution of selected features to the radiomics score for different outcome prediction (total recurrence, local recurrence, and distant metastasis). The features are plotted on the y-axis, their rescaled coefficients according to absolute values are plotted on the x-axis.

recurrence risk was significantly higher than that of the low-risk group (Odds ratio 16.25 and 0.06, respectively; $p < 0.001$). When the different CP risk factors were taken into account, recurrence-free survival time was always significantly longer in the low-risk group compared to that of the high-risk group (Fig. 5).

Combined Predictive Models and Comparison

The best CP predictor was the pTNM stage with lower AIC values for each outcome (TR, LR, DM; AIC = 487, 221, 268, respectively); therefore, only pTNM stage contributed to the final CP model. Radiomics signature outperformed TNM stage in predicting each outcome (Cox coefficient and p values: RS_{TR} = 0.74, 0.006; TNM_{TR} = 0.24, 0.016; RS_{LR} = 0.60, 0.035; TNM_{LR} = 0.22, 0.110; RS_{DM} = 0.71, 0.005; TNM_{DM} =0.25, 0.068). The best predictive model resulted from the combination of RS with the TNM stage (AUC_{TR} 0.760; AUC_{DM} 0.759; AUC_{LR} 0.750), when compared to the RS-only and TNM stage-only models for each outcome (Table 4). DeLong's test showed significant ROC curve differences between the single or combined models for all three outcomes (TR, LR, DM; p value = 0.01, 0.05, 0.01, respectively).

Nomograms confirmed that RS was played a substantial role in the risk scoring system compared to the TNM stage (Fig. 6). The calibration plots presented a good agreement for 1-, 2-, and 3-year end-points, which showed the reliability of the defined models for each outcome (Fig. 7).

DISCUSSION

In this study, we generated an RS by employing tumoral and peritumoral lung parenchyma features to predict postsurgical recurrence risk in NSCLC patients. We found that the identified signature is an independent risk predictor, and we were able to use the RS to stratify patient population in low- and high-risk groups. We demonstrated the added incremental value of the RS with respect to the TNM staging in individualized recurrence risk prediction.

Our proposed RS consisted of morphological (flatness, least axis length), intensity based (90th percentile) and textural (Grey level co-occurrence matrix, Grey level run length matrix, Grey level size zone matrix) features, which depict tumor shape and heterogeneity beyond the CT semantic characteristics (7–9). Tumor shape irregularities and intratumoral heterogeneity determined by the texture analysis was found to be successful predictors of patient survival (5,7–9,23,29,30). Tumor heterogeneity, caused by genomic instability, hypoxia, and angiogenesis, reflects the tumor aggressiveness and it accounts for differences in patient survival or treatment response (7,23).

Lymphovascular tumor invasion and micrometastasis, which are not directly discernible by the standard diagnostic imaging techniques, into peritumoral parenchyma play a crucial role in tumor recurrence (31,32). The presence of peritumoral interstitial thickening, determined as a semantic feature

TABLE 3. Selected Features, their Coefficients and RAD-Score Cut-Off Values for Each Outcome

Outcome	Selected Radiomics Features	Coefficients (95% CI)	Rad-score Cut-off (Youden Index)
Total recurrence	F_morph.pca.flatness.peritumor	3.15 (−0.967,7.267)	9.68
	F_cm.inv.var.peritumor	25.6 (8.577,42.623)	
	F_stat.90thpercentile.gtv	0.0043 (0.00018, 0.00842)	
	F_szm.glnu.norm.peritumor	−43.13 (−77.869,−8.391)	
Local recurrence	F_morph.pca.flatness.gtv	−5.55 (−12.26, 1.16)	−14.9
	F_rlm.rl.entr.gtv	−1.87 (−4.344, 0.604)	
	F_zsm.z.perc.gtv	32.7 (16.152, 49.248)	
	F_morph.av.gtv	−11.3 (−17.535,−5.065])	
	F_stat.var.gtv	0.000025 (0.0000054, 0.0000446)	
Distant metastasis	F_cm.inv.var.peritumor	16.60 (−4.996, 38.196)	22.09
	F_rlm.srhge.gtv	0.0092 (0.002, 0.016)	
	L_least.gtv	0.16 (0.057, 0.263)	
	F_rlm.lrhge.gtv	0.00059 (0.000159, 0.00102)	
	F_rlm.sre.gtv	11.17 (−1.023, 23.363)	

A suffix was added to feature names to keep track of the ROI that they referred to (peritumor or tumor (gtv)).
CI, confidence interval; pTNM, pathological tumor-node-metastasis; Rad-score, radiomics signature based score; ROI, region of interest.

on CT images, was found positively correlated to lymphovascular tumor invasion and tumor recurrence in NSCLC patients (3). Furthermore, a preliminary study showed that a combined evaluation of peritumoral semantic and tumoral radiomics features could improve risk prediction of the nodal involvement in NSCLC (10).

Peritumoral radiomics analyses, which were conducted on other cancer types, provided promising results due to their

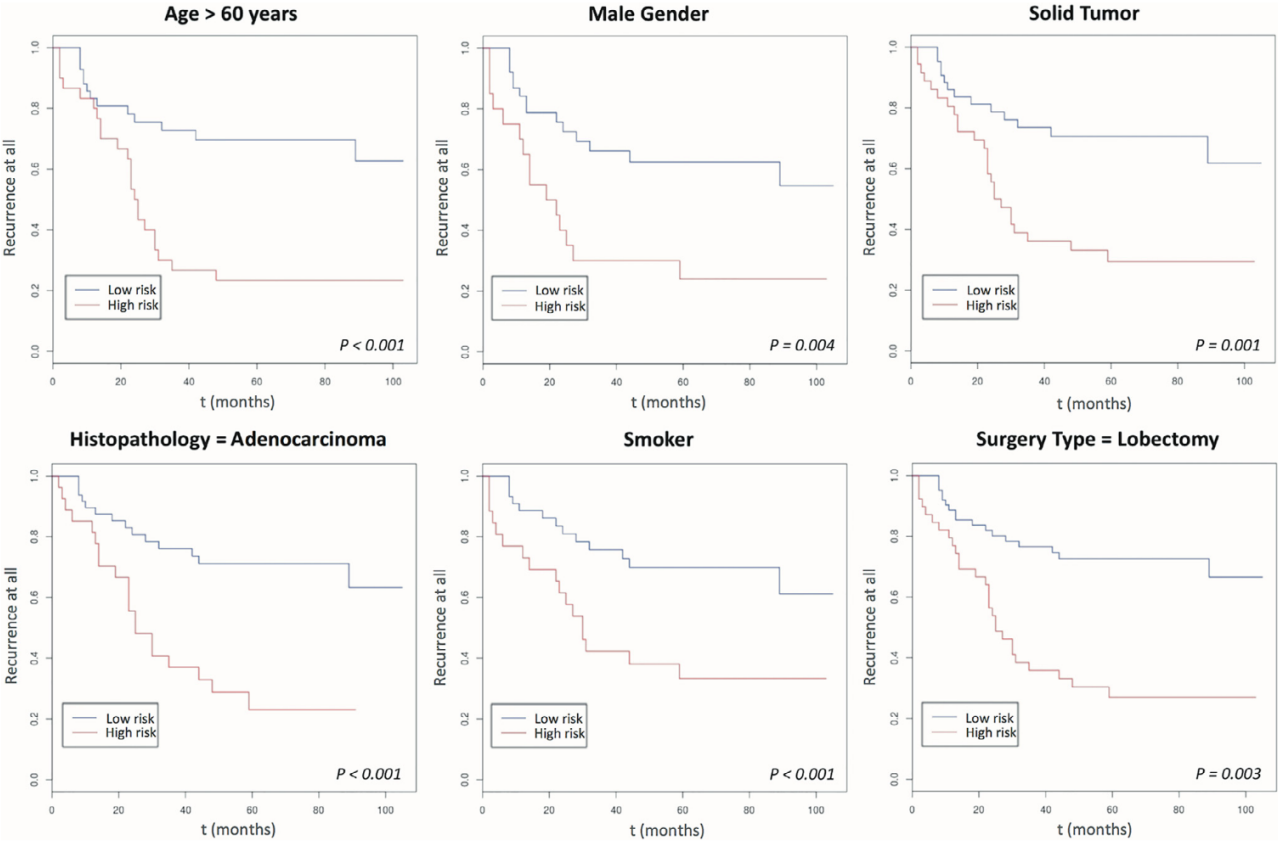

Figure 5. Graphics show the result of Kaplan-Meier curves of the survival analysis in patients stratified according to radiomics score by different clinicopathologic risk factors. The total recurrence outcome is plotted on the y-axis, time (months) since diagnosis is plotted on the x-axis.

TABLE 4. Radiomics Signature, Clinicopathologic (pTNM stage) and Combined Model Performances

Model	AUC (95% CI)	C−Index (SD)	AIC
Radiomics signature-only			
TR	0.750 (0.668, 0.832)	0.673 (0.041)	482
LR	0.731 (0.613, 0.849)	0.720 (0.060)	207
DM	0.750 (0.642, 0.858)	0.726 (0.055)	258
pTNM stage-only			
TR	0.680 (0.596, 0.764)	0.653 (0.043)	487
LR	0.580 (0.457, 0.703)	0.594 (0.063)	221
DM	0.672 (0.559, 0.785)	0.697 (0.058)	268
Radiomics signature + pTNM stage			
TR	0.760 (0.670, 0.850)	0.694 (0.046)	477
LR	0.750 (0.632, 0.868)	0.670 (0.060)	206
DM	0.759 (0.640, 0.878)	0.765 (0.061)	257

AIC, Akaike information criteria; AUC, area under the curve; CI, confidence interval; pTNM, pathological tumor-node-metastasis; SD, standard deviation.

capability to capture the infiltration of tumor cells into the surrounding breast tissue or cell proliferation and neovascularization in the peritumoral brain parenchyma (33,34). In two recent studies, peritumoral radiomics features, extracted from the vicinity of tumor boundary on pretreatment CT and positron emission tomography images, successfully predicted distant metastasis in locally advanced NSCLC and early-stage NSCLC treated with stereotactic body radiation therapy, respectively (11,12). In the former study, authors demonstrated that the "tumor exterior" (defined as the lung tissue extending from 3 mm to 9 mm outside of the tumor contour) is less predictive than the "tumor rim" (defined as the lung tissue located 3 mm away from the tumor contour) radiomics analysis (11). The safe surgical margin is accepted as 2 cm away from the tumor contour in an inflated lung, and in surgically treated patients, surgical margin less than 1 cm is found to be correlated with higher recurrence rates when compared to a surgical margin more than 1 cm (13,35). These studies emphasize the potential boundaries of tumor cell dissemination into the peritumoral lung tissue and its relation to tumor recurrence. Therefore, in our study, peritumoral radiomics features were extracted from the surgically defined safe margin, and we found that even 2 cm away from the tumor tissue carries valuable predictive information. Our predictive models, which are combination of peritumoral and tumoral RS, were substantial predictors of distant metastasis as well as of LR. To the best of our knowledge, our study is the first one considering quantitative peritumoral safe margin radiomics analysis along with tumoral radiomics analysis in predicting overall NSCLC outcome showing the added value of the identified RS to multiparametric nomograms.

The TNM staging system is the traditional method of stratifying patients at different prognoses, upon which the clinical decision-making on the treatment of NSCLC is based. However, differences in the outcome often exist among patients in the same clinical disease stage (6). Post-treatment survival prediction by employing tumoral radiomics analysis has already been on the focus of some studies (6,8,9). Radiomics features were found to be beneficial for pathological response prediction in patients with locally advanced NSCLC who received neoadjuvant chemo-/radiotherapy (8). In another study, when RS is combined with clinical covariates, the model was found to be a successful predictor of the overall survival and distant metastasis in patients with locally advanced adenocarcinoma (9). Moreover, tumor RS was described as a predictor of disease-free survival in patients with early-stage NSCLC, and the predictive performance of RS improved when TNM stage and other CP data (e.g., age, sex, histologic grade) were added to the predictive model (6). In line with these previous studies, the RS we identified in our study successfully stratified NSCLC patients in different risk groups, and recurrence risk prediction improved when

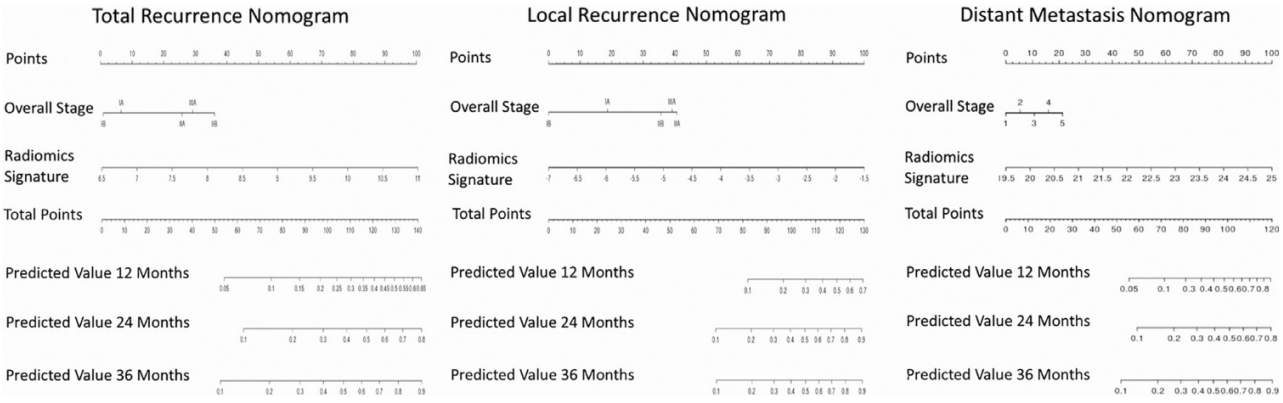

Figure 6. Nomograms developed with radiomics signature and TNM stage for total recurrence, local recurrence, and distant metastasis outcomes. First, locate the patient's TNM stage score on the second line and the radiomics signature score on the third line, then draw a line straight upward to the first line to ascertain how many points the patient receives for each score. Add the points and locate the final sum on the "Total Point" axis. Lastly draw a line straight down to the predicted value at 12, 24, or 36 months to estimate patient's probability of recurrence at target time-point.

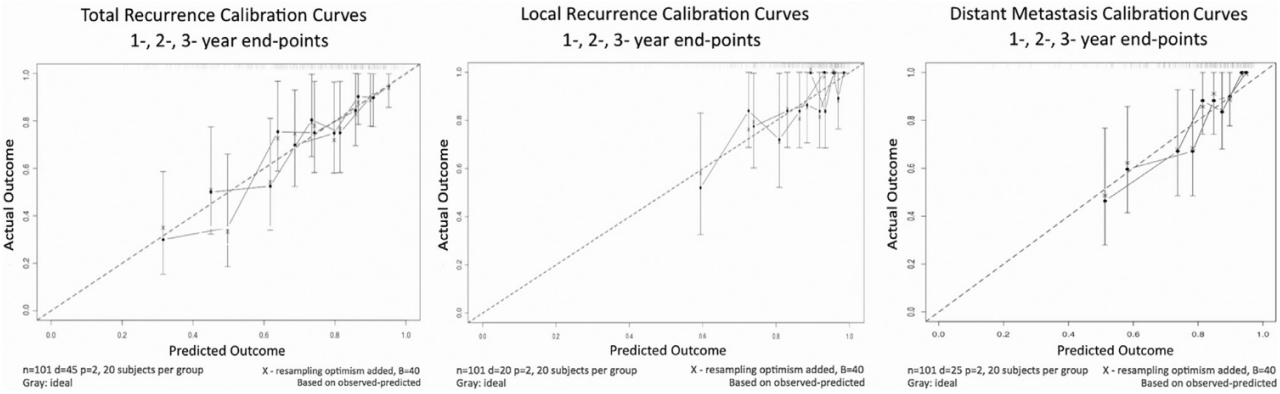

Figure 7. Calibration curves for the total recurrence, local recurrence, and distant metastasis nomograms at 1-, 2-, and 3-year end-points. The x-axis shows nomogram-estimated recurrence; the y-axis shows the observed recurrence. The diagonal dotted line depicts the perfect estimation by an ideal model. The solid lines depict performance of the nomogram. A closer interpolated solid lines to the diagonal dotted line represents a better estimation.

RS was combined with the TNM staging. In our study population, 13 out of 16 patients were upstaged at pathology due to microscopic lymph node metastases. Among them, patients who manifested recurrence (11 patients) were all classified as high-risk patients according to their RS. While their clinical TNM stage underestimated the risk of recurrence, their RS clearly showed that they were indeed included in the high-risk group. Thus, presurgical RS could predict prognosis better than clinical TNM staging alone in patients with microscopic lymph node metastases. Those patients enrolled in a higher stage have received the appropriate treatment only after surgery; therefore, they might have lost the critical time of treatment for having a better outcome. The hidden information in pretreatment images could be revealed with radiomics analysis, which could help us to personalize the treatment at the time of diagnosis.

As pictorial representations of statistical models, nomograms are often used in oncology and they take into account multiple risk factors to predict prognosis and to support clinical decision-making. Radiomics analysis of tumors allows obtaining measurable data that can be implemented in nomograms (6,36,37). While clinicopathologic-only nomograms predicted the overall/disease-free survival or lymph node metastasis better than the TNM staging alone, the nomograms with RS also demonstrated an incremental value in respect to the TNM staging system alone for individualized disease-free survival or lymph node metastasis estimation in NSCLC patients (6,37). Our nomograms with RS followed the same trend and added incremental value to the TNM staging system for individualized recurrence risk prediction.

The main limitations of our study are the retrospective nature of the collected data and the lack of external validation. Further studies with prospective design and external validation are required before widespread implementation of the presented RS and nomograms in the clinical practice. Another limitation is that our study population was small and heterogeneous regarding the tumor stage and histopathology. We found significantly higher recurrence rates in the higher stage tumors, as expected, but no significant recurrence differences between the different histopathological subgroups. The TNM 7th edition was used in clinical practice at the time of the disease staging in our population; therefore, we took into account this edition to built our predictive models. Our proposed model should be adapted to the current TNM 8th edition before clinical implementation.

We attributed the lung parenchyma peritumoral changes to the tumoral spread. However, 69% of our patients were smokers and the potential coexistence of smoking-related diffuse lung disease (e.g., interstitial lung disease, pulmonary emphysema) might have affected the extracted features from the peritumoral lung parenchyma. Therefore, further studies addressing the influence of smoking-related diffuse lung diseases on radiomics characteristics are needed to generate a more comprehensive risk prediction model.

In conclusion, our results showed that RS generated from the tumor and peritumoral lung parenchyma on presurgical CT images has the potential to predict recurrence in surgically treated NSCLC patients. The incremental value of our radiomics analysis over the traditional TNM staging prognostic system indicates that such RS could be a beneficial tool for the accurate presurgical risk stratification and a potential mean for practicing effective personalized treatment in NSCLC patients.

ACKNOWLEDGMENTS

This research did not receive any specific grant from funding agencies in the public, commercial, or nonprofit sectors.

Tugba Akinci D'Antonoli received a scholarship from the European School of Radiology in the form of a Thoracic Radiology Research Fellowship from 2016 to 2017 at Fondazione Policlinico Universitario "A. Gemelli" IRCCS, Dipartimento Diagnostica per Immagini, Radioterapia Oncologica ed Ematologia, Università Cattolica del Sacro Cuore, Istituto di Radiologia, Rome, Italy.

REFERENCES

1. Torre LA, Bray F, Siegel RL, et al. Global cancer statistics, 2012. CA Cancer J Clin 2015; 65:87–108.
2. Postmus PE, Kerr KM, Oudkerk M, et al. Early and locally advanced non-small-cell lung cancer (NSCLC): ESMO Clinical Practice Guidelines for diagnosis, treatment and follow-up. Ann Oncol 2017; 28(Suppl_4):iv1–iv21.
3. Koo HJ, Xu H, Choi C-M, et al. Preoperative CT predicting recurrence of surgically resected adenocarcinoma of the lung. Medicine 2016; 95: e2513.
4. McWilliams A, Tammemagi MC, Mayo JR, et al. Probability of cancer in pulmonary nodules detected on first screening CT. N Engl J Med 2013; 369:910–919.
5. Gillies RJ, Kinahan PE, Hricak H. Radiomics: images are more than pictures, they are data. Radiology 2016; 278:563–577.
6. Huang Yanqi, Liu Zaiyi, He Lan, et al. Radiomics signature: a potential biomarker for the prediction of disease-free survival in early-stage (I or II) non−small cell lung cancer. Radiology 2016; 281:947–957.
7. Mattonen SA, Tetar S, Palma DA, et al. Imaging texture analysis for automated prediction of lung cancer recurrence after stereotactic radiotherapy. J Med Imaging 2015; 2:041010.
8. Coroller TP, Agrawal V, Narayan V, et al. Radiomic phenotype features predict pathological response in non-small cell lung cancer. Radiother Oncol J 2016; 119:480–486.
9. Coroller TP, Grossmann P, Hou Y, et al. CT-based radiomic signature predicts distant metastasis in lung adenocarcinoma. Radiother Oncol 2015; 114:345–350.
10. Liu Y, Kim J, Balagurunathan Y, et al. Prediction of pathological nodal involvement by CT-based radiomic features of the primary tumor in patients with clinically node-negative peripheral lung adenocarcinomas. Med Phys 2018; 45:2518–2526.
11. Dou TH, Coroller TP, Van Griethuysen JJM. Peritumoral radiomics features predict distant metastasis in locally advanced NSCLC. PLoS One 2018; 13:e0206108.
12. Hao H, Zhou Z, Li S, et al. Shell feature: a new radiomics descriptor for predicting distant failure after radiotherapy in non-small cell lung cancer and cervix cancer. Phys Med Biol 2018; 63:1–17.
13. Ginsberg RJ, Rubinstein LV, Lung Cancer Study Group. Randomized trial of lobectomy versus limited resection for T1 N0 non-small cell lung cancer. Ann Thorac Surg 1995; 60:615–623.
14. Edge S, Byrd DR, Compton CC, Fritz AG, Greene F, Trotti A, eds. AJCC Cancer Staging Handbook [Internet], 7th ed., New York, NY: Springer; 2010. XIX, 718. XIX, 718.
15. Lardinois D, De Leyn P, Van Schil P, et al. ESTS guidelines for intraoperative lymph node staging in non-small cell lung cancer. Eur J Cardio-thoracic Surg 2006; 30:787–792.
16. Altorki NK, Yip R, Hanaoka T, et al. Sublobar resection is equivalent to lobectomy for clinical stage 1A lung cancer in solid nodules. J Thorac Cardiovasc Surg 2014; 147:754–764.
17. Zhao B, Tan Y, Tsai W-Y, et al. Reproducibility of radiomics for deciphering tumor phenotype with imaging. Sci Rep 2016; 6:23428.
18. Lu L, Ehmke RC, Schwartz LH, et al. Assessing agreement between radiomic features computed for multiple CT imaging settings. PLoS One 2016; 11:e0166550.
19. Parmar C, Velazquez ER, Leijenaar R, et al. Robust radiomics feature quantification using semiautomatic volumetric segmentation. PLoS One 2014; 9:e102107.
20. Gu Y, Kumar V, Hall LO, et al. Automated delineation of lung tumors from CT images using a single click ensemble segmentation approach. Pattern Recognit 2013; 46:692–702.
21. Balagurunathan Y, Kumar V, Gu Y, et al. Test−retest reproducibility analysis of lung CT image features. J Digit Imaging 2014; 27:805–823.
22. Kido S, Kuriyama K, Higashiyama M, et al. Fractal analysis of internal and peripheral textures of small peripheral bronchogenic carcinomas in thin-section computed tomography: comparison of bronchioloalveolar cell carcinomas with nonbronchioloalveolar cell carcinomas. J Comput Assist Tomogr 2003; 27:56–61.
23. Ganeshan B, Panayiotou E, Burnand K, et al. Tumour heterogeneity in non-small cell lung carcinoma assessed by CT texture analysis: a potential marker of survival. Eur Radiol 2012; 22:796–802.
24. Zwanenburg A, Leger S, Vallières M. et al. Initiative for the IBS. Image biomarker standardisation initiative. 2016. Available via: http://arxiv.org/abs/1612.07003. Accessed May 3 2019.
25. Dinapoli N, Alitto AR, Vallati M, et al. Moddicom: a complete and easily accessible library for prognostic evaluations relying on image features. IEEE Eng Med Biol Soc 2015: 771–774.
26. Aleksander SJ, Paclawski A, Lau R, et al. Heuristic modeling of macromolecule release from PLGA microspheres. Int J Nanomedicine 2013; 8:4601–4611.
27. Harrell FE. Regression modeling strategies. New York, NY: Springer-Verlag, 2015.
28. Ruopp MD, Perkins NJ, Whitcomb BW, et al. Youden index and optimal cut-point estimated from observations affected by a lower limit of detection. Biometrical J 2008; 50:419–430.
29. Yoon SH, Park CM, Park SJ, et al. Tumor heterogeneity in lung cancer: assessment with dynamic contrast-enhanced MR imaging. Radiology 2016; 280:940–948.
30. Grove O, Berglund AE, Schabath MB, et al. Quantitative computed tomographic descriptors associate tumor shape complexity and intratumor heterogeneity with prognosis in lung adenocarcinoma. PLoS One 2015; 10:e0118261.
31. Yang HC, Kim HR, Jheon S, et al. Recurrence risk-scoring model for stage I adenocarcinoma of the lung. Ann Surg Oncol 2015; 22:4089–4097.
32. Mollberg NM, Bennette C, Howell E, et al. Lymphovascular invasion as a prognostic indicator in stage I non-small cell lung cancer : a systematic review and meta-analysis. Ann Thorac Surg 2014; 97:965–971.
33. Prasanna P, Patel J, Partovi S, et al. Radiomic features from the peritumoral brain parenchyma on treatment-naïve multi-parametric MR imaging predict long versus short-term survival in glioblastoma multiforme: preliminary findings. Eur Radiol 2016; 27:4188–4197.
34. Braman NM, Etesami M, Prasanna P, et al. Intratumoral and peritumoral radiomics for the pretreatment prediction of pathological complete response to neoadjuvant chemotherapy based on breast DCE-MRI. Breast Cancer Res 2017; 19:1–14.
35. El-Sherif A, Fernando HC, Santos R, et al. Margin and local recurrence after sublobar resection of non-small cell lung cancer. Ann Surg Oncol 2007; 14:2400–2405.
36. Liang W, Deng Q, Zhang L, et al. Development and validation of a nomogram for predicting survival in patients with resected non − small-cell lung cancer. J Clin Oncol 2015; 33:861–869.
37. Kirienko M, Cozzi L, Antunovic L, et al. Prediction of disease-free survival by the PET/CT radiomic signature in non-small cell lung cancer patients undergoing surgery. Eur J Nucl Med Mol Imaging 2017; 45:207–217.